Millimeter-Wave Massive Arrays for Indoor SLAM

Francesco Guidi, Anna Guerra, and Davide Dardari
DEI, University of Bologna, via Venezia 52, I-47521 Cesena (FC), Italy
email: {anna.guerra3,f.guidi,davide.dardari}@unibo.it

***Abstract*—The adoption of millimeter waves will give the possibility to integrate massive antenna arrays inside next generation tablets and smartphones, with consequent significant enhancement of their communication performance. Besides communication, the availability of such a technology can also enable other interesting applications such as personal radar for accurate simultaneous localization and mapping (SLAM). In this paper we investigate the feasibility of 3D environment mapping for SLAM applications at millimeter waves exploiting massive antenna arrays on the user's mobile device. Frequency selectivity and phase quantization effects are accounted for to characterize the achievable angle and range resolution necessary to collect environmental 3D information under transmission power and scanning time constraints.**

***Index Terms*—Massive arrays, SLAM, millimeter-waves, beam steering, personal radar**

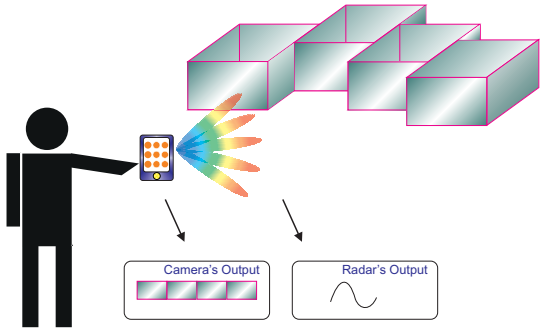

Fig. 1. Example of a SLAM scenario, where a tablet/smartphone, equipped with a massive antenna array, scans an environment.

I. Introduction

The idea of simultaneous localization and mapping (SLAM) is becoming more and more fascinating and it is supposed in the next years to be more spread, especially in the context of Internet of Things, where each object of interest is expected to be mapped into the Internet space for real time detection and information exchange [1]. Traditionally, SLAM is based on the concept that a robot, moving in an unknown environment, recognizes the surrounding objects being then able to reconstruct a 3D map of the area. This is typically done by steering a laser beam across a dense number of test directions and estimating the round-trip time (RTT) of the signal reflected by the obstacles (targets) for each test direction. In such a way, from RTT estimates, the distance of targets can be inferred and, consequently, a 3D map of the environment can be built. Accurate SLAM requires both high-definition distance estimates (ranging) and very narrow steering beams (angle resolution), such characteristics easily accomplished by laser technology. In [2] the state of the art of SLAM technology is described.

Unfortunately, high-accuracy SLAM technologies, based on laser and mechanical steering devices, do not allow an easy and low-cost integration in mobile devices. To overcome this drawback, the idea to combine millimeter-wave radars and SLAM has been considered [3], [4]. It is known that millimeter-wave radars provide accurate range measurements thanks to the high temporal resolution, and might overcomes the shortcomings of laser. Of particular interest for fifth generation (5G) mobile wireless communications in indoor environments is the 60 GHz band which allows the exploitation of a large clean unlicensed bandwidth (up to 7 GHz). The high atmospheric absorption at 60 GHz makes communication systems less susceptible to external interference [5]. The reduced wavelength at millimeter-waves paves the way for packing a large number of antenna elements into a small area and the adoption of massive arrays systems in base stations or access points [6], thus enabling improvements in terms of data rate, communication reliability, energy efficiency, and interference mitigation [7].

Stimulated by this possibility, in this paper we put forth the idea of placing massive antenna arrays in a smartphone or tablet, thus realizing a personal radar enabling SLAM features, in addition to communication data. The availability of a large number of antennas on mobile devices opens the possibility of realizing pencil beams with electronic-driven steering capabilities that are fundamental for high-accuracy SLAM applications as a cheap, energy efficient alternative to laser technology (see Fig. 1). Specifically, the narrow beam is steered towards a high number of test directions the 3D area is divided into. For each direction the RTT of the signal reflected backward by the target is measured from which the distance is estimated (ranging). In this way, by integrating the angle/range information collected during the scanning process with that coming from the conventional smartphone's embedded camera, it is possible to realize a pictorial 3D mapping of the surrounding area.

In this paper we analyze the steering and ranging capability of the proposed solution as a function of the signal bandwidth and the number of antennas composing the array. At millimeter waves unpractical and costly time-delay circuits must be avoided in favor of simpler digitally-controlled phase shifters. Therefore, the loss of steering and ranging accuracy

978-1-4799-4640-2/14/$31.00 ©2014 IEEE

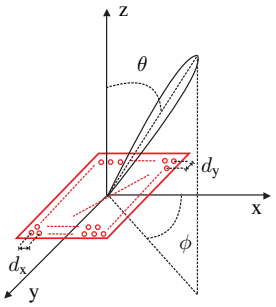

Fig. 2. Plan Array Configuration.

due to quantized phase shifters and frequency selectivity is also investigated.

II. Massive Antenna Arrays

The planar array configuration, exploiting the scanning properties of phased antenna arrays, appears well suited for massive antennas integration in smartphones and tablets. Consider the scheme reported in Fig. 2, where $N_{\text{array}} = MN$ antenna elements are placed in a rectangular area of dimension $L_x \times L_y$, with $L_x = Md_x$ and $L_y = Nd_y$. The elements are spaced apart of d_x (d_y) in the x (y) dimension. According to [8], the array factor (AF) at frequency f is defined as

$$\text{AF}(\Theta, f) = \sum_{m=1}^{M}\sum_{n=1}^{N} \omega_{mn} \cdot e^{j(m-1)(kd_x \sin\theta\, \cos\phi)} e^{j(n-1)(kd_y \sin\theta\, \sin\phi)} \quad (1)$$

with $\Theta = (\theta, \phi)$ being the considered direction identified by the elevation and the azimuthal angles, θ and ϕ, respectively, and $k = 2\pi f/c$ the wavenumber, with c indicating the speed of light.

The complex weights $\{\omega_{mn}\}$ determine the beam shape and pointing direction and can be expressed in general as

$$\omega_{mn} = a_{mn} e^{j\varphi_{mn}} = a_{mn} e^{j[(m-1)\beta_x + (n-1)\beta_y]} \quad (2)$$

where a_{mn} and φ_{mn} are, respectively, the weight's amplitude and phase, and β_x and β_y are the parameters set to steer the main array lobe towards the test pointing direction $\Theta_0 = (\theta_0, \phi_0)$.

Considering a uniform array (i.e. $a_{mn} = 1$), the AF becomes

$$\text{AF}(\Theta, f) = \sum_{m=1}^{M}\sum_{n=1}^{N} e^{j\left[(m-1)\widetilde{\Psi}_x + (n-1)\widetilde{\Psi}_y\right]} \quad (3)$$

with

$$\widetilde{\Psi}_x = kd_x \sin(\theta)\cos(\phi) + \beta_x \quad (4)$$

$$\widetilde{\Psi}_y = kd_y \sin(\theta)\sin(\phi) + \beta_y. \quad (5)$$

To steer the main lobe towards a specific direction Θ_0, parameters β_x and β_y have to be set to

$$\beta_x = -k_0 d_x \sin(\theta_0)\cos(\phi_0) \quad (6)$$

$$\beta_y = -k_0 d_y \sin(\theta_0)\sin(\phi_0) \quad (7)$$

with $k_0 = 2\pi f_0/c$, and f_0 being the reference frequency for which the steering parameters are designed. In the steering direction and for $f = f_0$, in the absence of non-idealities, it is $\text{AF}(\Theta_0, f_0) = MN = N_{\text{array}}$.

III. Sources of Error in Antenna Arrays

There are several issues that arise when massive wideband phased arrays are adopted and accurate beam steering and ranging have to be guaranteed. They are even more pronounced in case of massive arrays at very high frequencies due to technological and cost constraints [9].

This section deals with the effects of phase quantization errors and large signal bandwidth. The joint impact of such sources of error results in beam pointing errors, beamwidth spread, and signal combining power loss.

A. Large Signal Bandwidth

Large bandwidths are in general desirable thanks to the corresponding achievable high ranging resolution [10]. However, in a wideband system, the received signal arrives at each antenna element with a delay that is not negligible compared to the signal duration, and hence it cannot be compensated by only adopting phase shifters, as typically done in narrowband systems. Unfortunately, the adoption of a huge number of time delay circuits represents a high-cost solution, especially at millimeter frequencies, then phase shifters remain at the moment the most suitable solution [11]. Consequently, in the absence of time delays, the accumulation of the component received by each branch will result in a signal distortion. In other words, the actual steering direction and beamwidth would depend on frequency (beam squinting). For this reason the effects of signal bandwidth have to be carefully accounted for. On the other hands, if we want to make frequency selectivity effects negligible, the signal duration T_w has to verify the following condition:

$$T_w > \frac{L_x \sin\theta_0 \cos\phi_0 + L_y \sin\theta_0 \sin\phi_0}{c}. \quad (8)$$

This implies a constraint for the array (signal) bandwidth given by $W < 1/T_w$ which could reduce the ranging accuracy of the system.

B. Array Weights Errors

Even the adoption of high resolution analog phase shifters might still not be a feasible solution for millimeter waves massive arrays if we aim at keeping a low architecture cost. Digitally controlled phase shifters implementing a discrete set of phase shifts represent a cheaper alternative at the expense of quantization errors. Some new solutions have been investigated in [9] to find a compromise between the number of elements and the phase shifters accuracy.

Starting from the general model for the quantized version $\tilde{\omega}_{mn}$ of weights ω_{mn} adopted in [12] we express $\tilde{\omega}_{mn} = \omega_{mn} e^{j\delta_{mn}}$, with $|\omega_{mn}| = 1$, and δ_{mn} being zero-mean independent Gaussian random variables (RVs) with variance σ_δ^2. Note that array weights errors affect the beam steering accuracy and, consequently, the beamwidth. In addition, the

imperfect alignment of pulses at each array element causes temporal spread if it is not well counteracted. These effects can reduce the mapping accuracy in terms of angle and ranging resolution.

IV. Impact of Errors on Pointing and Angle Resolution

Denote with $\widetilde{\mathrm{AF}}(\Theta, f)$ the actual AF in the presence of the aforementioned errors. Expression (3) becomes

$$\widetilde{\mathrm{AF}}(\Theta, f) = \sum_{m=1}^{M}\sum_{n=1}^{N} e^{j\left[(m-1)\widetilde{\Psi}_{\mathrm{x}}+(n-1)\widetilde{\Psi}_{\mathrm{y}}\right]} e^{j\delta_{mn}} \tag{9}$$

where δ_{mn} are the phase errors previously defined. By considering small phase errors, i.e., $\delta_{mn} \ll 1$, we can write

$$\begin{aligned}|\widetilde{\mathrm{AF}}(\Theta, f)|^2 &= \sum_{m=1}^{M}\sum_{n=1}^{N}\sum_{p=1}^{M}\sum_{q=1}^{N} e^{j\left[(m-p)\widetilde{\Psi}_x+(n-q)\widetilde{\Psi}_y\right]} e^{j(\delta_{mn}-\delta_{pq})} \\ &\approx \sum_{mnpq} e^{j\left[(m-p)\widetilde{\Psi}_x+(n-q)\widetilde{\Psi}_y\right]}(1+\delta_{mn}\delta_{pq})\end{aligned} \tag{10}$$

where $\sum_{mnpq} = \sum_{m=1}^{M}\sum_{n=1}^{N}\sum_{p=1}^{M}\sum_{q=1}^{N}$. In the following we will discuss about the two effects that arise when (10) is considered. First, there is a beam pointing error, that is the array beam is no more exactly steered in the desired direction Θ_0 obtained at the reference frequency f_0. Second, the beamwidth changes in accordance with the joint influence of phase errors and squint effect.

1) Beam Pointing Error: Ideally, in the steering direction and under the hypothesis of uniformly excited weights, it is $|\mathrm{AF}(\Theta_0, f_0)|^2 = N^2_{\text{array}}$.

Now denote with $\widetilde{\Theta}_0 = (\tilde{\theta}_0, \tilde{\phi}_0)$ the actual beam pointing direction at frequency f. In the presence of non-ideal effects, the actual pointing direction can be evaluated by solving

$$\begin{aligned}S(\widetilde{\Theta}_0, f) &= \left.\frac{\partial|\widetilde{\mathrm{AF}}(\Theta, f)|^2}{\partial\theta}\right|_{\Theta=\widetilde{\Theta}_0} = 0 \\ F(\widetilde{\Theta}_0, f) &= \left.\frac{\partial|\widetilde{\mathrm{AF}}(\Theta, f)|^2}{\partial\phi}\right|_{\Theta=\widetilde{\Theta}_0} = 0\end{aligned} \tag{11}$$

Considering the expansion with the first order of the Taylor series evaluated in Θ_0, it is

$$\begin{aligned}&S(\widetilde{\Theta}_0, f) = \\ &= S(\Theta_0+\Delta\Theta_0, f) = S(\Theta_0, f) + \delta\tilde{\theta}_{\mathrm{BS}}\left.\frac{\partial S(\Theta, f)}{\partial\theta}\right|_{\Theta=\Theta_0} = 0 \\ &F(\widetilde{\Theta}_0, f) = \\ &= F(\Theta_0+\Delta\Theta_0, f) = F(\Theta_0, f) + \delta\tilde{\phi}_{\mathrm{BS}}\left.\frac{\partial F(\Theta, f)}{\partial\phi}\right|_{\Theta=\Theta_0} = 0\end{aligned} \tag{12}$$

where $\Delta\Theta_0 = (\delta\tilde{\theta}_{\mathrm{BS}}(\Theta_0, f), \delta\tilde{\phi}_{\mathrm{BS}}(\Theta_0, f)) = (\tilde{\theta}_0-\theta_0, \tilde{\phi}_0-\phi_0)$ is the steering angle deviation. Thus the solutions are

$$\begin{aligned}\delta\tilde{\theta}_{\mathrm{BS}}(\Theta_0, f) &= \frac{-S(\Theta_0, f)}{\left.\frac{\partial S(\Theta, f)}{\partial\theta}\right|_{\Theta=\Theta_0}}, \\ \delta\tilde{\phi}_{\mathrm{BS}}(\Theta_0, f) &= \frac{-F(\Theta_0, f)}{\left.\frac{\partial F(\Theta, f)}{\partial\phi}\right|_{\Theta=\Theta_0}}\end{aligned} \tag{13}$$

According to the approached followed in [12], we approximate the derivatives in (13) with their respective mean values, which allow us to write the mean square beam pointing error as

$$\begin{aligned}\mathbb{E}\left[\delta\tilde{\theta}^2_{\mathrm{BS}}(\Theta, f)\right] &= \left.\frac{\mathbb{E}\left[S^2(\Theta, f)\right]}{\left(\mathbb{E}\left[\frac{\partial S(\Theta, f)}{\partial\theta}\right]\right)^2}\right|_{\Theta=\Theta_0} \\ \mathbb{E}\left[\delta\tilde{\phi}^2_{\mathrm{BS}}(\Theta, f)\right] &= \left.\frac{\mathbb{E}\left[F^2(\Theta, f)\right]}{\left(\mathbb{E}\left[\frac{\partial\mathbb{E}[F(\Theta, f)]}{\partial\phi}\right]\right)^2}\right|_{\Theta=\Theta_0}.\end{aligned} \tag{14}$$

We focus our attention on the computation of the mean square beam pointing error in (14). First of all we find that

$$S(\Theta, f) = j\sum_{mnpq} e^{j\tilde{\alpha}_{mnpq}}(1+\delta_{mn}\delta_{pq})\frac{\partial\tilde{\alpha}_{mnpq}}{\partial\theta} \tag{15}$$

where we have introduced $\tilde{\alpha}_{mnpq} = (m-p)\widetilde{\Psi}_x + (n-q)\widetilde{\Psi}_y$ and

$$\frac{\partial\tilde{\alpha}_{mnpq}}{\partial\theta} = k\cos(\theta)\left[(m-p)d_x\cos(\phi)+(n-q)d_y\sin(\phi)\right]. \tag{16}$$

Taking the derivatives of (15), we have

$$\begin{aligned}&\frac{\partial S(\Theta, f)}{\partial\theta} = \\ &= j\sum_{mnpq} e^{j\tilde{\alpha}_{mnpq}}(1+\delta_{mn}\delta_{pq})\left[\frac{\partial^2\tilde{\alpha}_{mnpq}}{\partial\theta^2}+j\left(\frac{\partial\tilde{\alpha}_{mnpq}}{\partial\theta}\right)^2\right]\end{aligned} \tag{17}$$

with

$$\frac{\partial^2\tilde{\alpha}_{mnpq}}{\partial\theta^2} = -k\sin(\theta)\left[(m-p)d_x\cos(\phi)+(n-q)d_y\sin(\phi)\right] \tag{18}$$

Evaluating the expectation we obtain

$$\begin{aligned}&\mathbb{E}^2\left[\frac{\partial S(\Theta, f)}{\partial\theta}\right] = \\ &-\left\{\sum_{mnnp} e^{j\tilde{\alpha}_{mnpq}}\left[\frac{\partial^2\tilde{\alpha}_{mnpq}}{\partial\theta^2}+j\left(\frac{\partial\tilde{\alpha}_{mnpq}}{\partial\theta}\right)^2\right]\right\}^2\end{aligned} \tag{19}$$

as $\mathbb{E}\left[\delta_{mn}\delta_{pq}\right] \neq 0$ only when $(m=p,\, n=q)$ and $\tilde{\alpha}_{mnmn} = 0$. Analogously, it is

$$\begin{aligned}\mathbb{E}\left[S^2(\Theta, f)\right] &= -\left\{\sum_{mnpq} e^{j\tilde{\alpha}_{mnpq}}\left(\frac{\partial\tilde{\alpha}_{mnpq}}{\partial\theta}\right)\right\}^2 \\ &-2\sigma^4_\delta\sum_{mnpq}\left[e^{j\tilde{\alpha}_{mnpq}}\left(\frac{\partial\tilde{\alpha}_{mnpq}}{\partial\theta}\right)\right]^2.\end{aligned} \tag{20}$$

Similarly, the relations along ϕ are obtained following the same approach for θ, and the final expressions of the mean

$$\mathbb{E}\left[\delta\tilde{\theta}^2_{\text{BS}}(\Theta_0,f)\right]=-\frac{\left\{\sum_{mnpq}e^{j\tilde{\alpha}_{mnpq}}\left(\frac{\partial\tilde{\alpha}_{mnpq}}{\partial\theta}\right)\right\}^2+2\sigma_\delta^4\sum_{mnpq}\left[e^{j\tilde{\alpha}_{mnpq}}\left(\frac{\partial\tilde{\alpha}_{mnpq}}{\partial\theta}\right)\right]^2\Big|_{\Theta=\Theta_0}}{\left\{\sum_{mnnp}e^{j\tilde{\alpha}_{mnpq}}\left[\frac{\partial^2\tilde{\alpha}_{mnpq}}{\partial\theta^2}+j\left(\frac{\partial\tilde{\alpha}_{mnpq}}{\partial\theta}\right)^2\right]\right\}^2\Big|_{\Theta=\Theta_0}} \tag{21}$$

$$\mathbb{E}\left[\delta\tilde{\phi}^2_{\text{BS}}(\Theta_0,f)\right]=-\frac{\left\{\sum_{mnpq}e^{j\tilde{\alpha}_{mnpq}}\left(\frac{\partial\tilde{\alpha}_{mnpq}}{\partial\phi}\right)\right\}^2+2\sigma_\delta^4\sum_{mnpq}\left[e^{j\tilde{\alpha}_{mnpq}}\left(\frac{\partial\tilde{\alpha}_{mnpq}}{\partial\phi}\right)\right]^2\Big|_{\Theta=\Theta_0}}{\left\{\sum_{mnnp}e^{j\tilde{\alpha}_{mnpq}}\left[\frac{\partial^2\tilde{\alpha}_{mnpq}}{\partial\phi^2}+j\left(\frac{\partial\tilde{\alpha}_{mnpq}}{\partial\phi}\right)^2\right]\right\}^2\Big|_{\Theta=\Theta_0}} \tag{22}$$

square beam pointing error results are reported in (21) and (22).

Given the transmitted signal power spectral density (PSD) $P_{\text{t}}(f)$, with bandwidth W, we define the pointing root mean square error (PRMSE) as

$$\mathsf{PRMSE}(\Theta_0)=\sqrt{\frac{\int_W P_{\text{t}}(f)\mathbb{E}\left[\delta\tilde{\theta}^2_{\text{BS}}(\Theta_0,f)\right]\mathbb{E}\left[\delta\tilde{\phi}^2_{\text{BS}}(\Theta_0,f)\right]df}{\int_W P_{\text{t}}(f)df}}. \tag{23}$$

It will be shown in Sec. VI that small bandwidths W are better suited for high beam pointing accuracy. This is in contrast with the need to have large bandwidth signals for accurate ranging and a trade off has to be found as will be shown in the numerical results. It can also be easily verified from (9) that the quantization errors lead to an average power loss in the actual steering direction $\widetilde{\Theta}_0$ given by

$$\mathsf{PCLF}=\frac{N^2_{\text{array}}}{\mathbb{E}\left\{|\widetilde{\text{AF}}(\widetilde{\Theta}_0,f)|^2\right\}}=\frac{N^2_{\text{array}}}{N_{\text{array}}\left[1+(N_{\text{array}}-1)e^{-\sigma^2_\delta}\right]}\approx e^{\sigma^2_\delta} \tag{24}$$

also known as phase combining loss factor (PCLF).

2) Beamwidth Spread: We are now interested in finding the 3dB beamwidth spread $\widetilde{\Theta}_{\text{3dB}}=\left(\tilde{\theta}_0\pm\delta\theta,\tilde{\phi}_0\pm\delta\phi\right)$, which varies with the frequency. In particular, the half power beamwidth (HPBW) can be evaluated by solving the following equation

$$|\text{AF}(\widetilde{\Theta}_{\text{3dB}},f)|^2=\frac{1}{2}|\text{AF}(\widetilde{\Theta}_0,f)|^2 \tag{25}$$

It follows that

$$\sum_{mnpq}\hat{w}_{mnpq}e^{j(m-p)\Psi_{\delta x}}e^{j(n-q)\Psi_{\delta y}}e^{j(\delta_{mn}-\delta_{pq})}=$$
$$=\frac{1}{2}|\text{AF}(\widetilde{\Theta}_0,f)|^2 \tag{26}$$

where $\hat{w}_{mnpq}=e^{j\left[(m-p)\widetilde{\Psi}_x|_{\Theta=\widetilde{\Theta}_0}+(n-q)\widetilde{\Psi}_y|_{\Theta=\widetilde{\Theta}_0}\right]}$ and

$$\Psi_{\delta\text{x}}=kd_{\text{x}}\left[\cos(\tilde{\theta}_0)\cos(\tilde{\phi}_0)\delta\theta-\sin(\tilde{\theta}_0)\sin(\tilde{\phi}_0)\delta\phi\right]$$
$$\Psi_{\delta\text{y}}=kd_{\text{y}}\left[\sin(\tilde{\theta}_0)\cos(\tilde{\phi}_0)\delta\phi+\cos(\tilde{\theta}_0)\sin(\tilde{\phi}_0)\delta\theta\right]. \tag{27}$$

As a consequence, (26) can be rearranged by developing the first-order series expansion of $e^{j\left[(m-p)\Psi_{\delta_x}+(n-q)\Psi_{\delta_y}\right]}$

$$\sum_{mnpq}\hat{w}_{mnpq}e^{j\delta_{mnpq}}\Delta^2_{mnpq}=\sum_{mnpq}\hat{w}_{mnpq}e^{j\delta_{mnpq}} \tag{28}$$

where $\Delta_{mnpq}=(m-p)\Psi_{\delta x}+(n-q)\Psi_{\delta y}$, and $\delta_{mnpq}=\delta_{mn}-\delta_{pq}$. To derive the BSA we adopt an approach similar to that proposed in [8] and [13] where the beam is considered alternatively lying on the XZ- and YZ-plane.

Specifically, consider the case in which $\tilde{\phi}_0=0$ and $\delta\phi=0$ so that the beam lies on the XZ-plane, with deviation of $\pm\delta\theta_{x0}$ from the beam pointing direction in that plane. We have that $\Delta_{mnpq}=(m-p)kd_x\delta\theta_{x0}\cos(\tilde{\theta}_0)$ and (28) can be written as

$$\sum_{mnpq}\hat{w}_{mnpq}e^{j\delta_{mnpq}}(m-p)^2k^2d_x^2\delta\tilde{\theta}^2_{x0}\cos^2(\tilde{\theta}_0)=|\text{AF}(\widetilde{\Theta}_0,f)|^2. \tag{29}$$

It is possible to find

$$\delta\tilde{\theta}_{x0}(\widetilde{\Theta}_0,f)\approx\pm\left[\frac{|\text{AF}(\widetilde{\Theta}_0,f)|^2}{\sum_{mnpq}\hat{w}_{mnpq}(m-p)^2k^2d_x^2\cos^2(\tilde{\theta}_0)}\right]^{1/2} \tag{30}$$

where we approximated $e^{j\delta_{mnpq}}\approx 1$ in the denominator, giving

$$\delta\tilde{\theta}_{x0}(\widetilde{\Theta}_0,f)=\delta\theta_{x0}(\widetilde{\Theta}_0,f)\sqrt{1+\left(\frac{|\text{AF}(\widetilde{\Theta}_0,f)|^2}{N^2_{\text{array}}}-1\right)} \tag{31}$$

where

$$\delta\theta_{x0}(\widetilde{\Theta}_0,f)=\pm\left[\frac{N^2_{\text{array}}}{\sum_{mnpq}\hat{w}_{mnpq}(m-p)^2k^2d_x^2\cos^2(\tilde{\theta}_0)}\right]^{1/2}. \tag{32}$$

By developing (32) using a first-order series expansion we have

$$\delta\tilde{\theta}_{x0}(\widetilde{\Theta}_0,f)=\frac{\delta\theta_{x0}(\widetilde{\Theta}_0,f)}{2}\left(1+\frac{|\text{AF}(\widetilde{\Theta}_0,f)|^2}{N^2_{\text{array}}}\right) \tag{33}$$

with the expectation value given by

$$\mathbb{E}\left[\delta\tilde{\theta}_{x0}(\widetilde{\Theta}_0, f)\right] = \frac{\delta\theta_{x0}(\widetilde{\Theta}_0, f)}{2}\left(1 + \frac{1}{\mathsf{PCLF}}\right). \quad (34)$$

The second case is when the beam lies on the YZ-plane (when $\tilde{\phi}_0 = \pi/2$ and $\delta\phi = 0$). Following the same steps as before, we obtain

$$\mathbb{E}\left[\delta\tilde{\theta}_{y0}(\widetilde{\Theta}_0, f)\right] = \frac{\delta\theta_{y0}(\widetilde{\Theta}_0, f)}{2}\left(1 + \frac{1}{\mathsf{PCLF}}\right) \quad (35)$$

where

$$\delta\theta_{y0}(\widetilde{\Theta}_0, f) = \pm\left[\frac{N_{\text{array}}^2}{\sum_{mnpq}\hat{w}_{mnpq}(n-q)^2k^2d_y^2\cos^2(\tilde{\theta}_0)}\right]^{1/2}. \quad (36)$$

Finally, the beam solid area (BSA) is

$$\mathsf{BSA} = \Omega_{\text{A}}(\widetilde{\Theta}_0, f) = 4\,\mathbb{E}\left[\delta\tilde{\theta}_{x0}(\widetilde{\Theta}_0, f)\right]\mathbb{E}\left[\delta\tilde{\theta}_{y0}(\widetilde{\Theta}_0, f)\right]\sec\tilde{\theta}_0. \quad (37)$$

In addition, we can also define the *effective BSA* as

$$\Omega_{\text{A, eff}}(\Theta_0) = \sqrt{\frac{\int_W P_{\text{t}}(f)\Omega_{\text{A}}^2(\widetilde{\Theta}_0, f)df}{\int_W P_{\text{t}}(f)df}} \quad (38)$$

where this parameter gives the angle resolution of the scanning process.

V. Target Ranging

Target distance estimate (ranging) during each step of the scanning process is obtained through the measurement of the signal RTT. The fundamental limit of ranging accuracy of a target at distance r depends on the signal effective bandwidth W_{eff} and the received signal-to-noise ratio (SNR) as given by the Cramér-Rao lower bound (CRLB) [10]

$$\mathsf{CRLB} = \frac{c^2}{8\pi^2\mathsf{SNR}\,W_{\text{eff}}^2} \quad (39)$$

where W_{eff} is defined as

$$W_{\text{eff}} \triangleq \sqrt{\frac{\int_{-\infty}^{+\infty} f^2P_{\text{t}}(f)df}{\int_{-\infty}^{+\infty} P_{\text{t}}(f)df}} \approx W. \quad (40)$$

We evaluate in the following the SNR accounting for the planar array described in Sec. II. The millimeter-wave radar range equation related to a target at distance r, a test steering direction Θ_0, and considering a waveform with incident direction $\Theta_i = (\theta_i, \phi_i)$, can be expressed as

$$P_{\text{r}}(\Theta_0, \Theta_i, r) = \int_W \frac{P_{\text{t}}(f)G^2(\Theta_0, f)c^2\Sigma(\Theta_0, \Theta_i, f, r)}{(4\pi)^3\,r^4\,L_{\text{atm}}\,f^2}\,df \quad (41)$$

with $G(\Theta_0, f) \approx \pi^2/\Omega_{\text{A}}(\Theta_0, f)$, being the array gain [8],[1] $\Sigma(\Theta_0, \Theta_i, f, r)$ the target radar cross section (RCS), and L_{atm} accounting for the atmosphere absorption at millimeter waves.

[1]For simplicity and without loss of generality, we consider isotropic array elements.

Note that typical values of L_{atm} are around $7 - 15.5\,\text{dB}/\text{km}$ [14].

Under the narrow beamwidth hypothesis, we approximate the illuminated area on the target's surface with the beam area of the incident wave generated by the massive array. Thus, the RCS of a target at millimeter-waves is given by [15]

$$\Sigma(\Theta_0, \Theta_i, f, r) = 4\pi\rho A_{\text{fp}}(\Theta_0, f, r)\zeta(\Theta_i) \quad (42)$$

where ρ is a parameter which depends on the type of scattering and the target material, and $\zeta(\Theta_i)$ is the incident/reflection coefficient of the target in the direction Θ_i. The footprint area is

$$A_{\text{fp}}(\Theta, f, r) = \frac{\pi}{4}r^2\Omega_{\text{A}}(\Theta, f) \quad (43)$$

with $\Omega_{\text{A}}(\Theta, f)$ given by (37). Thus (42) becomes

$$\Sigma(\Theta_0, \Theta_i, f, r) = (\pi r)^2\,\Omega_{\text{A}}(\Theta_0, f)\,\rho\,\zeta(\Theta_i) \quad (44)$$

and (41) results

$$P_{\text{r}}(\Theta_0, \Theta_i, r) = \frac{\pi c^2}{64}\int_W \frac{\text{EIRP}(f)\,\rho\,\zeta(\Theta_i)}{L_{\text{atm}}\,r^2f^2}\,df, \quad (45)$$

where $\text{EIRP}(f) = P_{\text{t}}(f)G(\Theta_0, f)$ is the effective radiated isotropic power (EIRP) typically constrained by regulatory power emission limits. Note the quadratic dependency on the mobile-target distance r in (45), and that N_{array} enters $\Omega_{\text{A}}(\Theta_0, f)$.

The actual SNR can be improved by increasing the transmission power or the observation time (e.g., by transmitting several pulses/symbols). However, both parameters have some constraints, respectively, from spectrum emission regulations and the maximum tolerable scanning time. For what the latter is regarded, we assume we have to scan half of the full solid angle $\Omega_{\text{o}} = 4\pi$ [sr] using the array integrated in the mobile device. The overall time for completing a half three dimensional (3D) scan is

$$T_{\text{scan}} = \frac{\Omega_{\text{o}}}{2}\cdot\frac{T_{\text{obs}}}{\Omega_{\text{mean}}} = \frac{2\pi}{\Omega_{\text{mean}}}\cdot T_{\text{obs}} \quad (46)$$

where Ω_{mean} denotes the mean solid beam angle averaged over all the possible test directions Θ_0

$$\Omega_{\text{mean}} = \frac{1}{\Omega_{\text{o}}}\int_{\theta_0}\int_{\phi_0}\Omega_{\text{A,eff}}(\Theta_0)d\phi_0\,d\theta_0, \quad (47)$$

and with T_{obs} the observation time for each test direction. Note that the scanning time depends on the BSA; a narrow beam increases the scanning time, while the scanning angle resolution is improved. Under scanning time constraints, the SNR is given by

$$\mathsf{SNR} = \frac{P_{\text{r}}(\Theta_0, \Theta_i, r)T_{\text{obs}}}{N_0} = \frac{P_{\text{r}}(\Theta_0, \Theta_i, r)T_{\text{scan}}\Omega_{\text{mean}}}{2\pi N_0} \quad (48)$$

where $N_0 = N_{\text{array}}\kappa\cdot T_0\cdot F$, being κ the Boltzmann constant, $T_0 = 290\,[\text{K}]$ the receiver temperature, and F the receiver noise figure.

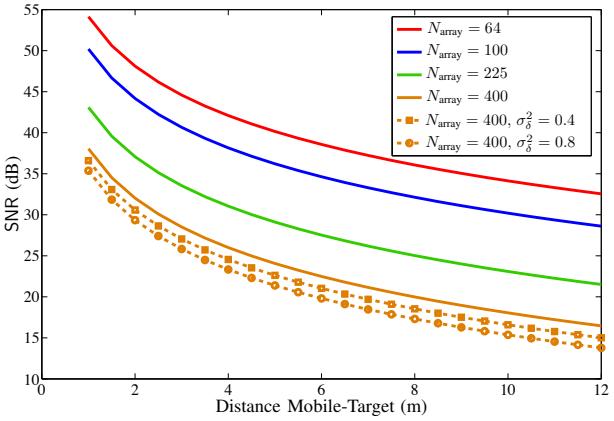

Fig. 3. SNR vs. mobile-target distance for different N_{array} values, $\Theta_0 = (45°, 45°)$, and $W = 500\,\text{MHz}$.

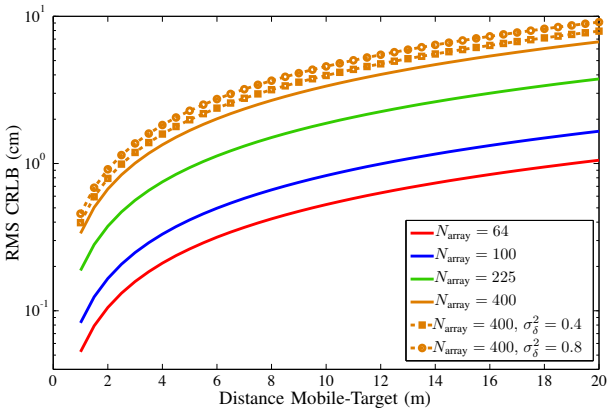

Fig. 4. RMS CRLB vs. mobile-target distance for different N_{array} values, $\Theta_0 = (45°, 45°)$, and $W = 500\,\text{MHz}$.

VI. Case Study

In this section we show some results with the planar array pattern considered. In the following, the system parameters are first described, and then numerical results are shown.

A. System Parameters

According to the wavelength λ and the object size L, there are different scattering regimes. Coherently with [16], we assume here to have $\lambda \ll L$ (optics regime) even if in some cases it could result in a rough approximation. We consider the approximation of a Lambertian scattering, adopting the laser model proposed in [15] for the monostatic laser RCS, where ρ is defined as $\rho = \rho_{\text{d}}/\pi$, with ρ_{d} being the diffuse reflectivity (albedo). We consider a target made of aerate concrete by approximating the albedo with the power reflection coefficient, evaluated by setting the concrete relative permittivity to $\epsilon_r = 2.26$ and its loss tangent to 0.0491 [17].

We consider a scanning time $T_{\text{scan}} = 1\,\text{ms}$, $F = 4\,\text{dB}$ and the transmission of a root raised cosine (RRC) signal compliant with the Federal Communications Commission (FCC) mask at 60 GHz ([18]), but with an average EIRP limited to 30 dBm as here we consider an handset device. Results are obtained for Θ_{i} normal to the target.

B. Numerical Results

Figure 3 shows SNRs curves obtained for different mobile-target distances and for different values of array elements N_{array}, where the transmitted signal bandwidth is set to $W = 500\,\text{MHz}$. When N_{array} increases, the SNR decreases due to the reduced BSA. In fact, according to (48) and the constraint on EIRP, N_{array} enters only N_0 and Ω_{mean}, which is inversely proportional to the massive arrive gain. Thus, large values of N_{array} improve the scanning angle resolution, but worsen the SNR. In addition, the presence of quantization errors degrades the SNR even if its impact is not serious. Note that for many array configurations SNR $>$ 15dB can be guaranteed for ranges up to 10 m.

The corresponding RMS CRLB on ranging is reported in Fig. 4. It is interesting to note that, as a consequence of the previous analysis, the ranging accuracy is reduced when the number of array elements is increased. On the contrary, the bandwidth improves the ranging accuracy, as shown in Fig. 5, but it has a detrimental effect on the PRMSE, as can be noticed in Fig. 6, which is very sensitive to the test elevation angle θ_0 but not to the phase errors considered. Thus there is a trade-off between the ranging accuracy, which improves with the bandwidth, and the array pointing error which also increases with W due to frequency selectivity effects. The bandwidth and the phase errors slightly affect the effective BSA and hence the scanning angle resolution, as can be observed in Fig. 7. On the contrary, we assist to a strong impact of N_{array} and the steering angle on the $\Omega_{\text{A, eff}}(\Theta_0)$. Such variations of the BSA affect both the SNR and the ranging accuracy, and need to be cautiously taken into account during the system design.

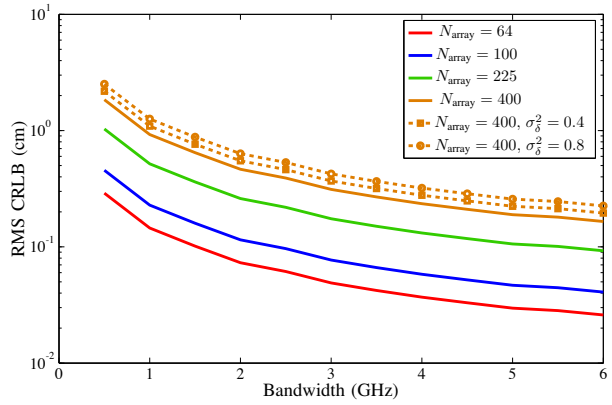

Fig. 5. RMS CRLB vs. transmitted signal bandwidth W for a mobile-target distance of 10 m.

From our preliminary results, arrays with about 100 elements and a signal bandwidth of $W = 1\,\text{GHz}$ seem a good compromise to obtain good scanning performance.

VII. Conclusions

We put forth the idea of adopting massive antenna arrays at millimeter-waves as an effective way to enable SLAM

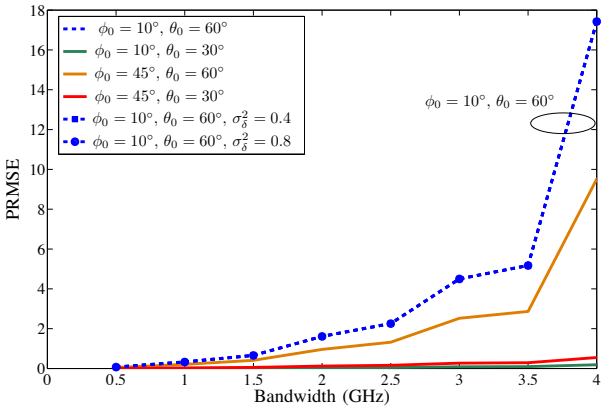

Fig. 6. PRMSE vs. signal bandwidth W for different test elevation angles, obtained with $N_{\text{array}}^2 = 100$.

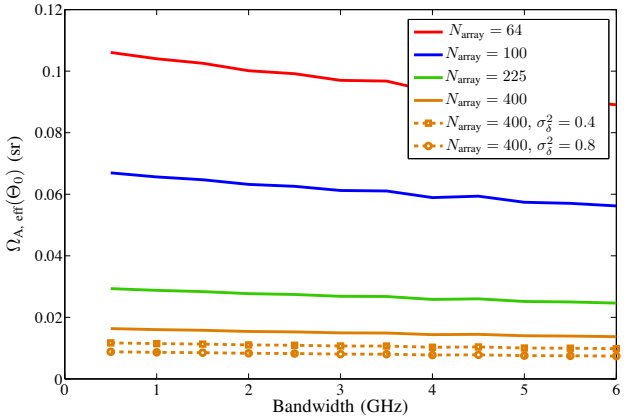

Fig. 7. Effective beam solid area vs. signal bandwidth W for $\Theta_0 = (45°, 45°)$.

applications using smartphones and tablets acting as personal radar. The quantization and frequency selectivity effects have been accounted for to derive the pointing error, the beamwidth spread and the ranging accuracy as a function of the number of antenna elements in the planar array. The analysis has highlighted how angle resolution, scanning time, signal bandwidth and ranging accuracy are tightly coupled and how a suitable trade off has to be achieved. Preliminary numerical results have shown the feasibility of the proposed idea in the 60 GHz band. The angle/distance information collected by the millimeter wave SLAM can be further combined with 2D textures from integrated cameras thus obtaining a realistic 3D mapping of the environment. This aspect is under investigation.

Acknowledgment

This work has been supported by the Italian Ministerial PRIN project GRETA (Grant 2010WHY5PR).

References

[1] C. Floerkemeier, M. Langheinrich, E. Fleisch, F. Mattern, and S. E. Sarma, Eds., *The Internet of Things, First Int. Conf.* Springer, 2008.

[2] H. Durrant-Whyte and T. Bailey, "Simultaneous localisation and mapping (SLAM): Part I the essential algorithms," *IEEE Robotics and Automation Mag.*, vol. 2, pp. 99–110, 2006.

[3] M. W. M. G. Dissanayake, P. Newman, S. Clark, H. F. Durrant-Whyte, and M. Csorba, "A solution to the simultaneous localization and map building (SLAM) problem," *IEEE Trans. on Robotics and Automation*, vol. 17, pp. 229–241, 2001.

[4] E. Jose and M. Adams, "An augmented state SLAM formulation for multiple line-of-sight features with millimetre wave radar," in *IEEE/RSJ International Conf. Intelligent Robots and Systems*, Aug. 2005, pp. 3087–3092.

[5] K. Dong, N. Prasad, X. Wang, and S. Zhu, "Adaptive antenna selection and Tx/Rx beamforming for large-scale MIMO systems in 60 GHz channels," *EURASIP Journal on Wireless Communications and Networking*, vol. 2011, no. 1, p. 59, 2011. [Online]. Available: http://jwcn.eurasipjournals.com/content/2011/1/59

[6] J. Hoydis, S. ten Brink, and M. Debbah, "Massive MIMO in the UL/DL of cellular networks: How many antennas do we need?" *IEEE J. Select. Areas Commun.*, vol. 31, no. 2, pp. 160–171, 2013.

[7] E. G. Larsson, F. Tufvesson, O. Edfors, and T. L. Marzetta, "Massive MIMO for next generation wireless systems," *CoRR*, vol. abs/1304.6690, 2013.

[8] C. Balanis, *Antenna Theory*, 3rd ed. Wiley, 2005.

[9] J. Krieger, C.-P. Yeang, and G. Wornell, "Dense delta-sigma phased arrays," *IEEE Trans. Antennas Propag.*, vol. 61, no. 4, pp. 1825–1837, 2013.

[10] D. Dardari, A. Conti, U. Ferner, A. Giorgetti, and M. Z. Win, "Ranging with ultrawide bandwidth signals in multipath environments," *Proc. of IEEE, Special Issue on UWB Technology & Emerging Applications*, vol. 97, no. 2, pp. 404–426, Feb 2009.

[11] P. Baltus, P. Smulders, and Y. Yu, *Systems and Architectures for Very High Frequency Radio Links*. Springer Netherlands, 2008.

[12] L. Rondinelli, "Effects of random errors on the performance of antenna arrays of many elements," in *IRE International Convention Record*, vol. 7, March 1959, pp. 174–189.

[13] R. S. Elliot, *Antenna Theory and Design*. New York: Prentice-Hall, 1981.

[14] F. Giannetti, M. Luise, and R. Reggiannini, "Mobile and personal communications in 60 GHz band: A survey," *Wirelesss Personal Comunications*, vol. 10, pp. 207–243, 1999.

[15] W. Wagner, "Radiometric calibration of small-footprint full-waveform airborne laser scanner measurements: Basic physical concepts," {*ISPRS*} *Journal of Photogrammetry and Remote Sensing*, vol. 65, no. 6, pp. 505 – 513, 2010.

[16] K. Sarabandi, E. Li, and A. Nashashibi, "Modeling and measurements of scattering from road surfaces at millimeter-wave frequencies," *IEEE Trans. Antennas Propagat.*, vol. 45, no. 11, pp. 1679–1688, Nov. 1997.

[17] L. Correia and P. Frances, "Estimation of materials characteristics from power measurements at 60 GHz," in *5th IEEE Intern. Symposium on Personal, Indoor and Mobile Radio Communications (PIRMC)*, 1994, pp. 510–513 vol.2.

[18] FCC, "Revision of Part 15 of the Commissions Rules Regarding Operation in the 57-64 GHz Band. August 2013."